Journal of Solid State Chemistry 183 (2010) 2582–2588

Contents lists available at ScienceDirect

Journal of Solid State Chemistry

journal homepage: www.elsevier.com/locate/jssc

Series of compositions $Bi_2(M'_xM_{1-x})_4O_9$ (M', M=Al, Ga, Fe; $0 \le x \le 1$) with mullite-type crystal structure: Synthesis, characterization and $^{18}O/^{16}O$ exchange experiment

T. Debnath [a,*], C.H. Rüscher [a], P. Fielitz [b], S. Ohmann [b], G. Borchardt [b]

[a] Institut für Mineralogie und Zentrum für Festkörperchemie und neue Materialien (ZFM), Leibniz Universität Hannover, Callinstraße 3, 30167 Hannover, Germany
[b] Institut für Metallurgie, Arbeitsgruppe Thermochemie und Mikrokinetik, TU Clausthal, Robert-Koch-Straße 42, 38676 Clausthal-Zellerfeld, Germany

ARTICLE INFO

Article history:
Received 27 February 2010
Received in revised form
16 June 2010
Accepted 10 July 2010
Available online 17 July 2010

Keywords:
Bismuth aluminum oxide
Bismuth gallium oxide
Bismuth iron oxide
Mullite-type structure
Bismuth compounds
FTIR spectra
$^{18}O_2$ tracer diffusion

ABSTRACT

Series of compositions $Bi_2(M'_xM_{1-x})_4O_9$ with x=0.0, 0.1,…, 1.0 and M'/M=Ga/Al, Fe/Al and Fe/Ga were synthesized by dissolving appropriate amounts of corresponding metal nitrate hydrates in glycerine, followed by gelation, calcination and final heating at 800 °C for 24 h. The new compositions with M'/M=Ga/Al form solid-solution series, which are isotypes to the two other series M'/M=Fe/Al and Fe/Ga. The XRD data analysis yielded in all cases a linear dependence of the lattice parameters related on x. Rietveld structure refinements of the XRD patterns of the new compounds, $Bi_2(Ga_xAl_{1-x})_4O_9$ reveal a preferential occupation of Ga in tetrahedral site (4 h). The IR absorption spectra measured between 50 and 4000 cm^{-1} of all systems show systematic shifts in peak positions related to the degree of substitution. Samples treated in $^{18}O_2$ atmosphere (16 h at 800 °C, 200 mbar, 95% $^{18}O_2$) for $^{18}O/^{16}O$ isotope exchange experiments show a well-separated IR absorption peak related to the M–$^{18}O_c$–M vibration, where O_c denotes the common oxygen of two tetrahedral type MO_4 units. The intensity ratio of M–$^{18}O_c/M$–$^{16}O_c$ IR absorption peaks and the average crystal sizes were used to estimate the tracer diffusion coefficients of polycrystalline $Bi_2Al_4O_9$ ($D=2\times10^{-22}$ m^2s^{-1}), $Bi_2Fe_4O_9$ ($D=5\times10^{-21}$ m^2s^{-1}), $Bi_2(Ga/Al)_4O_9$ ($D=2\times10^{-21}$ m^2s^{-1}) and $Bi_2Ga_4O_9$ ($D=2\times10^{-20}$ m^2s^{-1}).

1. Introduction

The crystal structure of $Bi_2M_4O_9$ type compounds with M=Al, Fe, Ga [1–3] belongs to the mullite-type family as was realized recently [4]. A characteristic feature represents the chains of edge-shared MO_6 octahedral type units extended along the c axis, which are linked by dimers (M_2O_7) of distorted MO_4 tetrahedral units, forming five-membered rings of two octahedra (MO_6) and three tetrahedra (MO_4) (Fig. 1). As a result, a channel-like structure is formed parallel to the octahedral chains, where Bi^{3+} ions are located. The BiO_4 groups alternate with the planes of M_2O_7 units, where the Bi $6s^2$ lone pairs point into the channels [5]. These materials exhibit interesting properties like photoluminescence [6–8] and significant oxygen ionic conductivity [9]. An anisotropic thermal expansion of $Bi_2Ga_4O_9$ single crystal has been reported by Filatov et al. [10]. Interestingly, enhanced one-dimensional oxygen diffusion has been proposed by Abrahams et al. [11] to occur along c axis.

Solid-solution series $Bi_2(Fe_xGa_{1-x})_4O_9$ [12] and $Bi_2(Fe_xAl_{1-x})_4O_9$ [13] were synthesized in order to tailor the physical properties of $Bi_2M_4O_9$ phases (M=Al, Ga, Fe). In so far there is no report on the preparation of $Bi_2(Ga_xAl_{1-x})_4O_9$ solid-solution series. This has incited us to prepare this new series. It may be noted that Belik et al. [14] prepared Bi_2O_3–Ga_2O_3–Al_2O_3 containing solid solutions $BiGa_xAl_{1-x}O_3$ using a high temperature/high-pressure technique at 6 GP and 1273–1473 K obtaining, however, perovskite type phases. In this work, we have prepared polycrystalline $Bi_2(Ga_xAl_{1-x})_4O_9$, $Bi_2(Fe_xAl_{1-x})_4O_9$ and $Bi_2(Fe_xGa_{1-x})_4O_9$ powder samples by dissolving the corresponding metal nitrate hydrate into glycerine and heating the formed gel at 800 °C for 24 h. This method follows that of Voll et al. [15] who also used an organic precursor method to prepare $Bi_2(Fe_xAl_{1-x})_4O_9$ solid-solution series. Some preliminary results obtained in the new system $Bi_2(Ga_xAl_{1-x})_4O_9$ were reported in contributions [16–18]. Here a detailed description of our results including XRD data will be given. IR absorption spectra of the new system, $Bi_2(Ga_xAl_{1-x})_4O_9$, in comparison to two other known systems $Bi_2(Fe_xAl_{1-x})_4O_9$ and $Bi_2(Fe_xGa_{1-x})_4O_9$ will be given, showing the systematic formation and variation of peak positions related to chemical substitution. Additionally, $^{18}O/^{16}O$ isotope exchange in combination with infrared absorption spectroscopy and XRD was used to investigate the oxygen diffusion of powder samples. This seems to be

* Corresponding author.
E-mail addresses: tapas.debnath@mineralogie.uni-hannover.de, tapasnet@yahoo.com (T. Debnath).

0022-4596/$ - see front matter © 2010 Elsevier Inc. All rights reserved.
doi:10.1016/j.jssc.2010.07.019

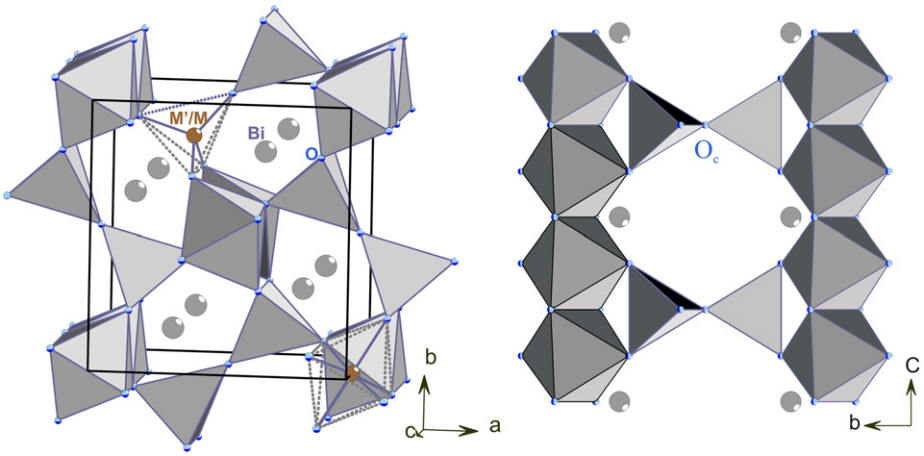

Fig. 1. Perspective views of the mullite-type $Bi_2M_4O_9$ unit cell (left) and showing the edge-shared octahedral type chains interconnected via M_2O_7 dimer units (right). Here O_c represents the common oxygen of two tetrahedral type MO_4 units.

necessary in order to obtain oxygen diffusion data since discussions about a possible significant oxygen conduction are based as yet on impedance spectroscopic data [9,19,20] and crystal structural considerations [5,11] only.

2. Experimental

It has been reported that the "Glycerine Method" should be the easiest synthesis technique to prepare pure single phase polycrystalline materials for the system $Bi_2(Fe_xAl_{1-x})_4O_9$ [15,21] compared to other methods e.g. "Glycine combustion technique" [20] or conventional solid state method [22]. Thus, the "Glycerine Method" is used here for the systematic synthesis of three solid-solution series $Bi_2(Fe_xAl_{1-x})_4O_9$, $Bi_2(Fe_xGa_{1-x})_4O_9$ and $Bi_2(Ga_xAl_{1-x})_4O_9$ with $x=0.0, 0.1, \ldots, 1.0$.

Aluminum nitrate 9-hydrate (Sigma-Aldrich), gallium nitrate 7-hydrate (Sigma-Aldrich), iron(III) nitrate hydrate, bismuth nitrate 5-hydrate (Sigma-Aldrich) and glycerine (Sigma-Aldrich) were used as raw materials to prepare $Bi_2(M'_xM_{1-x})_4O_9$ with M'/M=Ga/Al, Fe/Al, Fe/Ga and $x=0.0, 0.1,\ldots, 1.0$. Metal nitrates taken in the required stoichiometric ratio were mixed with glycerine (metal:glycerine=1:3). The mixture of the metal salts and glycerine was slowly heated at 80 °C to form a viscous gel and subsequently heated at 120 °C in a furnace for about 12 h. During this process the gel swells into a fluffy mass which eventually breaks up into brittle flakes. The dried gel was calcined in an open Pt crucible at 800 °C for about 24 h to get the final product. The amount of water in the hydrated nitrates was measured using TG (Setaram Setsys evolution 1750) and also from the weight loss after slow heating of hydrated nitrates at 600 °C in an open Pt crucible.

X-ray powder-diffraction data of $Bi_2(Ga_xAl_{1-x})_4O_9$ were collected at room temperature for $2\theta=15^\circ\ldots115^\circ$ using a Stoe Stadi P diffractometer (transmission geometry, Co$K\alpha_1$ radiation by a focusing Ge (1 1 1) monochromator, linear PSD). The normal-focus Co X-ray tube was operated at 35 kV and 40 mA. Profiles were taken with a 2θ step interval of 0.02°, counting time per step 120 s. The structures were refined with the Rietveld program Diffrac Plus TOPAS (Bruker AXS, Karlsruhe, Germany). The occupancy of M (M=Al, Ga) in the tetrahedral or octahedral sites was constrained so that $[Al]_{tetra/oct}=1-[Ga]_{tetra/oct}$. For the calculation of the reflex profiles fundamental parameters were used on the basis of instrumental parameters calculated from a silicon standard measurement. As an additional general parameter the zero point of the centre was varied and a polarization parameter was fixed.

Infrared absorption spectra were recorded on a Bruker Vertex 80 V FTIR spectrometer under vacuum. For the IR spectroscopic measurements (in the range of 370–4000 cm^{-1}) 1.0 mg of the finely ground sample was dispersed into 199.0 mg potassium bromide (KBr) and pressed into a pellet (13.0 mm diameter). The spectrum of a pure KBr (200.0 mg) pellet prepared in the same way was used as a reference. To measure the absorption spectra down to 50 cm^{-1}, polyethylene was used instead of KBr as a reference material. Using the overlapping range both spectra were merged together. Spectra are given in absorbance units ($-\log(I/I_0)$, where I_0, I are transmitted intensities through "reference" and "reference+sample", respectively).

To perform the $^{18}O/^{16}O$ exchange experiments, the samples were placed on an alumina holder and were then introduced into the cold zone of the furnace, which were subsequently evacuated to a pressure of about 10^{-3} mbar. After evacuation, the furnace was filled with 200 mbar $^{18}O_2$-enriched gas. The exact $^{18}O_2$ gas concentration in the furnace was measured by a residual gas analyser (RGA 200, Stanford Research Systems) to be 95% ^{18}O. A mechanical feed-through manipulator allowed to rapidly introduce the sample holder into the hot zone (800 °C) of the furnace, or to withdraw it, respectively. The heating period of the samples was 16 h.

3. Results and discussion

3.1. X-ray diffraction and Rietveld refinement

It is observed that all the X-ray diffraction peaks of all products can perfectly be indexed to the orthorhombic structure (space group=*Pbam*). The initial values of the lattice parameters used for the refinements were from Niizeki and Wachi [1] for $Bi_2Al_4O_9$ and from Müller-Buschbaum and de Beaulieu [3] for $Bi_2Ga_4O_9$. The refined lattice parameters for the end members of the new series agree well with the reported values. It is observed (Fig. 2) that the lattice parameters increase linearly as a function of x in all systems. The results of a linear regression analysis are given in Table 1. Compared to earlier reports for the Fe/Al and Fe/Ga systems there is a significant less scattering in the data, probably due to the improved synthesis technique. Abrahams et al. [11] prepared polycrystalline $Bi_2Al_4O_9$ by conventional solid state synthesis using equimolar amounts of corresponding oxides. These authors, however, reported about 6% α-Al_2O_3 as an

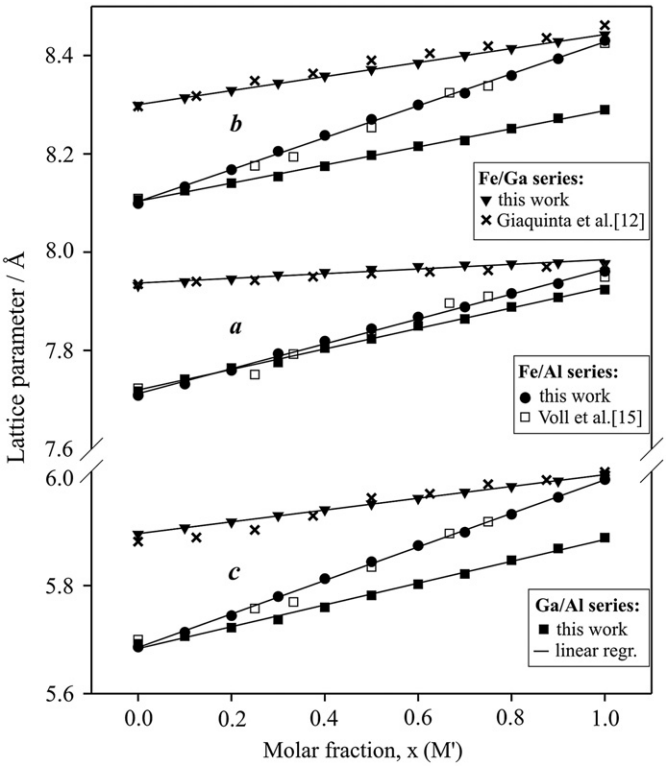

Fig. 2. Lattice parameters for the solid-solution series, $Bi_2(M'_xM_{1-x})_4O_9$, as a function of molar fraction $x(M')$. The solid triangles, circles and squares represent the lattice parameters of the $Bi_2(Fe_xGa_{1-x})_4O_9$, $Bi_2(Fe_xAl_{1-x})_4O_9$, and $Bi_2(Ga_xAl_{1-x})_4O_9$ series, respectively, synthesized in the present work. The solid lines represent the linear regression of the lattice parameters. The lattice parameters of $Bi_2(Fe_xGa_{1-x})_4O_9$ (cross symbols) and $Bi_2(Fe_xAl_{1-x})_4O_9$ (empty squares), taken from Giaquinta et al. [12] and Voll et al. [15], respectively, are also compared.

Table 1
Coefficients (m, p) of linear equation, $f(x)=mx+p$, obtained from the regression analysis of the lattice parameters of $Bi_2(M'_xM_{1-x})_4O_9$ solid-solution series.

System	Axis	m	p
$Bi_2(Ga_xAl_{1-x})_4O_9$	a	0.209	7.7194
	b	0.184	8.1036
	c	0.202	5.6835
$Bi_2(Fe_xAl_{1-x})_4O_9$	a	0.048	7.9371
	b	0.143	8.3001
	c	0.109	5.8962
$Bi_2(Fe_xGa_{1-x})_4O_9$	a	0.253	7.7121
	b	0.325	8.1028
	c	0.311	5.6853

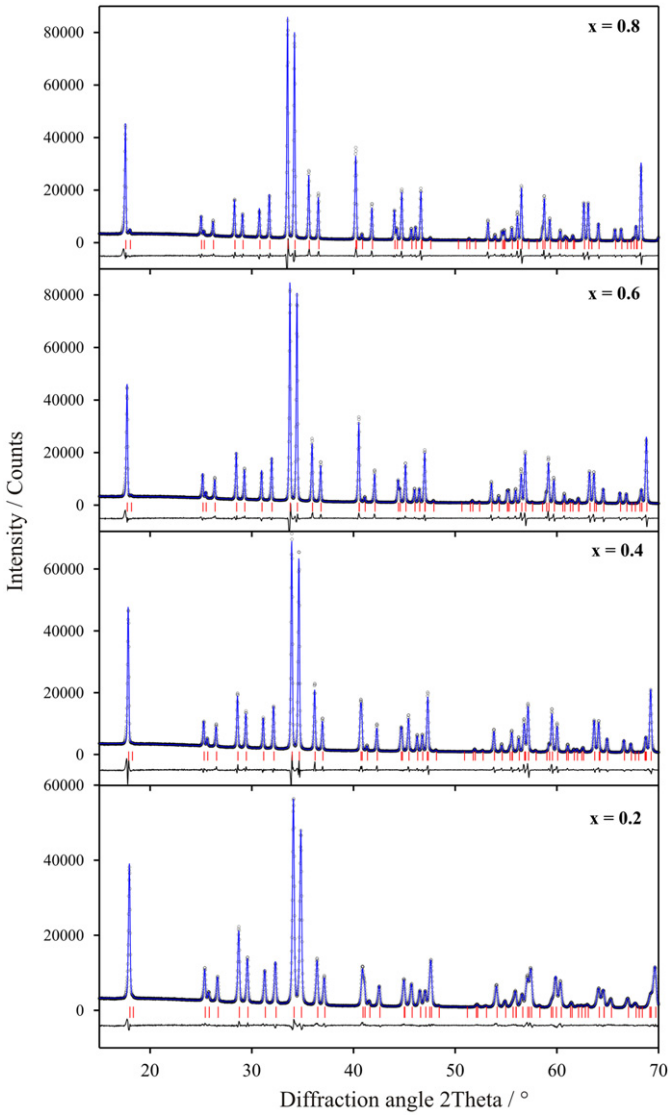

Fig. 3. Observed X-ray diffraction pattern (dotted, black) and calculated pattern (solid line, blue) using the Rietveld method for some of the selected samples of the $Bi_2(Ga_xAl_{1-x})_4O_9$ series. The respective difference curve and indexed peak positions (bars, red) are also shown. Rietveld refinements were done in whole measured range ($2\theta=10^\circ-115^\circ$), but for the sake of clarity the diffraction patterns are shown in the range of $2\theta=15^\circ-70^\circ$. (For interpretation of the references to colour in this figure legend, the reader is referred to the web version of this article.)

impurity phase. Larose and Akbar [19] reported the presence of $Bi_{24}Al_2O_{39}$ phase during the preparation of $Bi_2Al_4O_9$. The formation of impurity phases here could be due to the inhomogeneity of the initial oxide mixtures, which may be hard to avoid in conventional synthesis routes. Moreover, evaporation loss of Bi_2O_3 during calcination at high temperature is another factor. Such problems could be eliminated through the use of organic precursors in the synthesis route. Dissolving salts of the constituent cations into a proper organic solvent generally tend to decrease calcination temperature to reach the desired product. Therefore, an organic precursor method seems to be the most suitable method for synthesizing single phase multi-cation oxide powders at relatively low temperatures.

Fig. 3 shows the Rietveld refinement fit of some of the selected samples of the $Bi_2(Ga_xAl_{1-x})_4O_9$ solid-solution series. Details of data collection and structure refinement results of all samples are given in Table 2. The positional parameters and the site occupancies of selected samples ($x=0.4$, 0.6 and 0.8) obtained after Rietveld refinement have been published recently [18]. The results could be reproduced here including all samples ($x=0.1$, 0.2, …., 0.9). According to this, the positional parameters do not vary significantly with changing Ga/Al compositions. However, the site occupancy of Al and Ga in the tetrahedral or octahedral sites varies non-statistically as shown in Fig. 4. It is observed that the Ga^{3+} ions occupy the tetrahedral sites more frequently than the octahedral sites. This result is similar to that reported by Müller-Buschbaum and de Beaulieu [3] and by Giaquinta et al. [12] who reported a preferred occupation (60%) of Ga on tetrahedral sites in $Bi_2Ga_2Fe_2O_9$. Although non-statistical occupations on M^{3+} sites occur in the systems Fe/Ga and Ga/Al as also observed in the IR absorption spectra (see below) no

Table 2
Lattice parameters, unit cell volume and R, S, $D-W$ values for $Bi_2(Ga_xAl_{1-x})_4O_9$ series refined using space group *Pbam*.

x	0.0	0.1	0.2	0.3	0.4	0.5	0.6	0.7	0.8	0.9	1.0
a (Å)	7.71901(6)	7.7312(2)	7.75080(8)	7.7711(2)	7.79697(7)	7.8161(1)	7.83752(8)	7.85677(8)	7.88345(6)	7.90077(6)	7.9231(2)
b (Å)	8.10511(7)	8.1147(1)	8.12838(9)	8.1496(2)	8.16575(7)	8.1824(1)	8.20096(8)	8.21916(8)	8.24579(6)	8.26585(6)	8.2893(2)
c (Å)	5.68867(5)	5.70038(8)	5.71466(7)	5.7341(2)	5.75442(5)	5.77355(8)	5.79475(6)	5.81596(6)	5.84335(4)	5.86449(4)	5.88880(7)
V (Å^3)	355.902(5)	357.634(9)	360.032(7)	363.15(2)	366.33(7)	369.243(9)	372.439(7)	375.572(6)	379.816(5)	382.990(5)	386.765(8)
R_p	5.47	2.85	3.23	5.06	4.86	5.55	5.70	6.12	5.38	4.12	3.78
R_{wp}	7.13	3.71	4.23	6.81	6.68	7.66	8.11	8.81	7.45	5.51	5.24
R_{exp}	3.43	1.90	2.01	4.91	2.00	2.70	1.99	2.04	1.99	2.99	3.00
S	2.08	1.95	2.10	1.39	3.34	2.84	4.08	4.32	3.75	1.84	1.75
$D-W$	0.57	0.54	0.45	1.05	0.31	0.34	0.21	0.21	0.25	0.62	0.68

Note: Step interval (2θ) 10°–115°, step 0.02. R_p=R-pattern, R_{wp}=weighted-pattern, R_{exp}=R-expected, S (R_{wp}/R_{exp})=Goodness of fit and D–W=Durbin–Watson d-statistic.

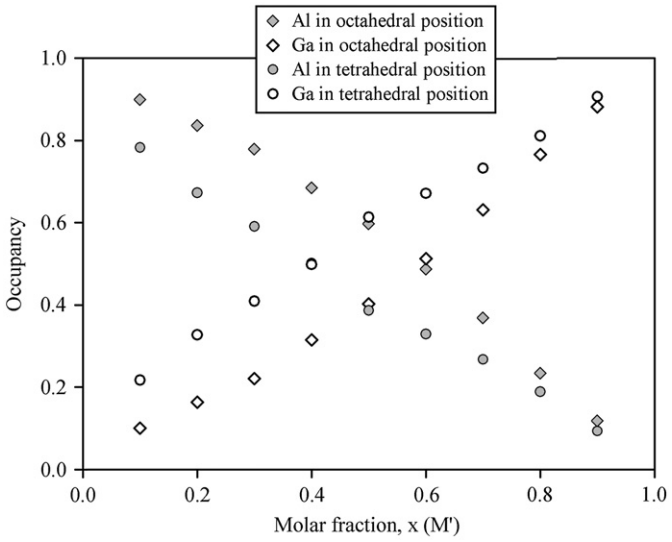

Fig. 4. Octahedral and tetrahedral occupancies of M (M=Ga, Al) in the $Bi_2(Ga_xAl_{1-x})_4O_9$ series, obtained from Rietveld refinement fit of XRD data.

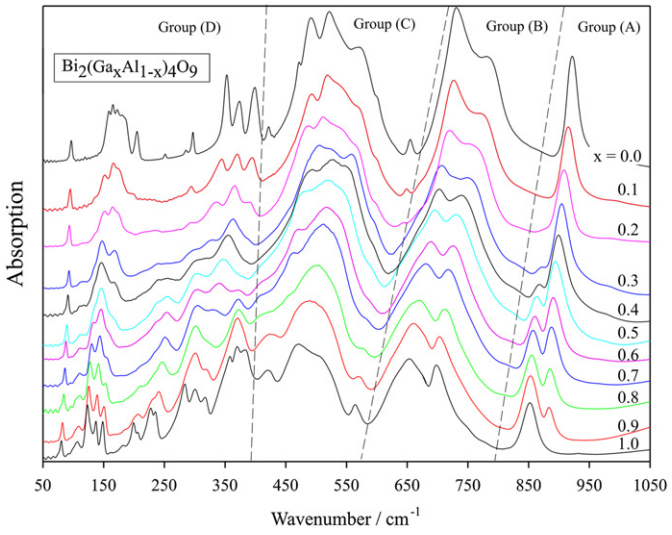

Fig. 5. IR absorption spectra of some selected samples of the $Bi_2(Ga_xAl_{1-x})_4O_9$ solid-solution series. The spectra are shifted vertically for the sake of clarity.

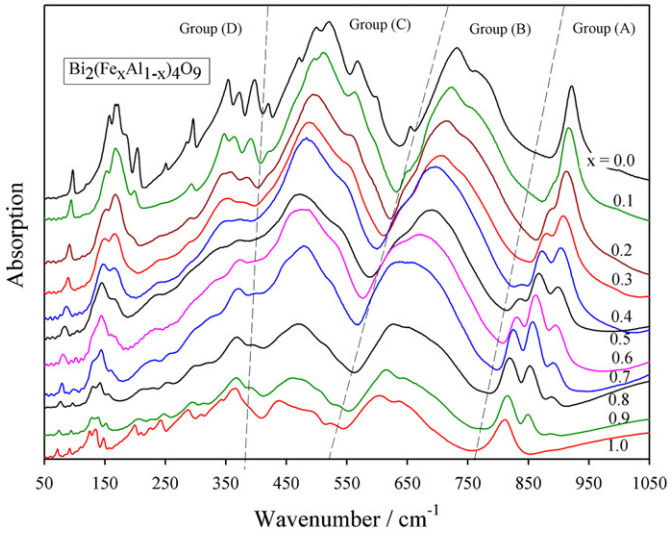

Fig. 6. IR absorption spectra of some selected samples of the $Bi_2(Fe_xAl_{1-x})_4O_9$ solid-solution series. The spectra are shifted vertically for the sake of clarity.

deviations for Vegards rules could be observed in the variation of lattice parameters (Fig. 2). Thus the co-efficients (m, p) of the linear equation ($f(x)=mx+p$) given in Table 1 can be used straightforward for the determination of M'/M ratios of $Bi_2(M'_xM_{1-x})_4O_9$ series using the absolute values of lattice parameters (a, b, c).

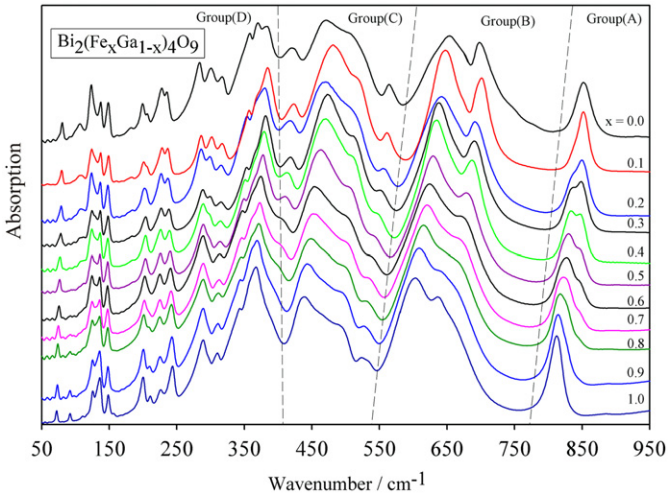

Fig. 7. IR absorption spectra of some selected samples of the $Bi_2(Fe_xGa_{1-x})_4O_9$ solid-solution series. The spectra are shifted vertically for the sake of clarity.

3.2. Infrared absorption spectra

IR absorption spectra of $Bi_2(M'_xM_{1-x})_4O_9$ with $x=0.0, 0.1,\ldots,$ 1.0 and M'/M=Ga/Al, Fe/Al and Fe/Ga solid-solution series are shown in the regions of 50–1100 cm^{-1} in Figs. 5–7, respectively. The spectra can be characterized by four distinct band groups following Voll et al. [15] (for end member $Bi_2Al_4O_9$) and Beran et al. [23] (for end member $Bi_2Ga_4O_9$), which were assigned to band group (A): M–O_c–M stretch (O_3M–O_c–MO_3 dimer); group (B)=M–O stretch (MO_4), M–O–M bend (MO_4); group (C)=O–M–O bend (MO_4), M–O stretch (MO_6), O–M–O bend (MO_6), M–O–M bend (MO_6) and group (D)=Bi–O vibrations. In case of $Bi_2Al_4O_9$, group (A–D) bands are centered in the 950–900, 820–680, 670–410 and 410–50 cm^{-1} regions, respectively. For $Bi_2Ga_4O_9$ and $Bi_2Fe_4O_9$ compounds, the bands of group (A–D) are centered in the regions of 880–820, 750–580, 580–400, 400–50 cm^{-1} and 840–770, 710–540, 540–400, 400–50 cm^{-1}, respectively. It is observed that the shift in peak positions between end members of binary systems $Bi_2(M'_xM_{1-x})_4O_9$ systematically increases for M'/M=Ga/Al, Fe/Ga and Fe/Al, respectively (compare Figs. 5–7).

Factor group analysis reveals for the compositions $Bi_2M_4O_9$ (space group *Pbam*) in total 36 IR active modes distributed according to 14 B_{3u} (E//a), 14 B_{2u} (E//b) and 8 B_{1u} (E//c) [23]. Using polarized single crystal reflectivity for $Bi_2Ga_4O_9$ spectra between 100 and 1200 cm^{-1} Beran et al. [23] could largely resolve 12, 12 and 6 peaks for the polarisations E//a, E//b and E//c, respectively. Some of the missing modes could be separated in the powder spectrum (Fig. 5) at 75 cm^{-1} (shoulder) and 79 cm^{-1} probably polarized within the (0 0 1) plane and at about 104 cm^{-1} (broad)

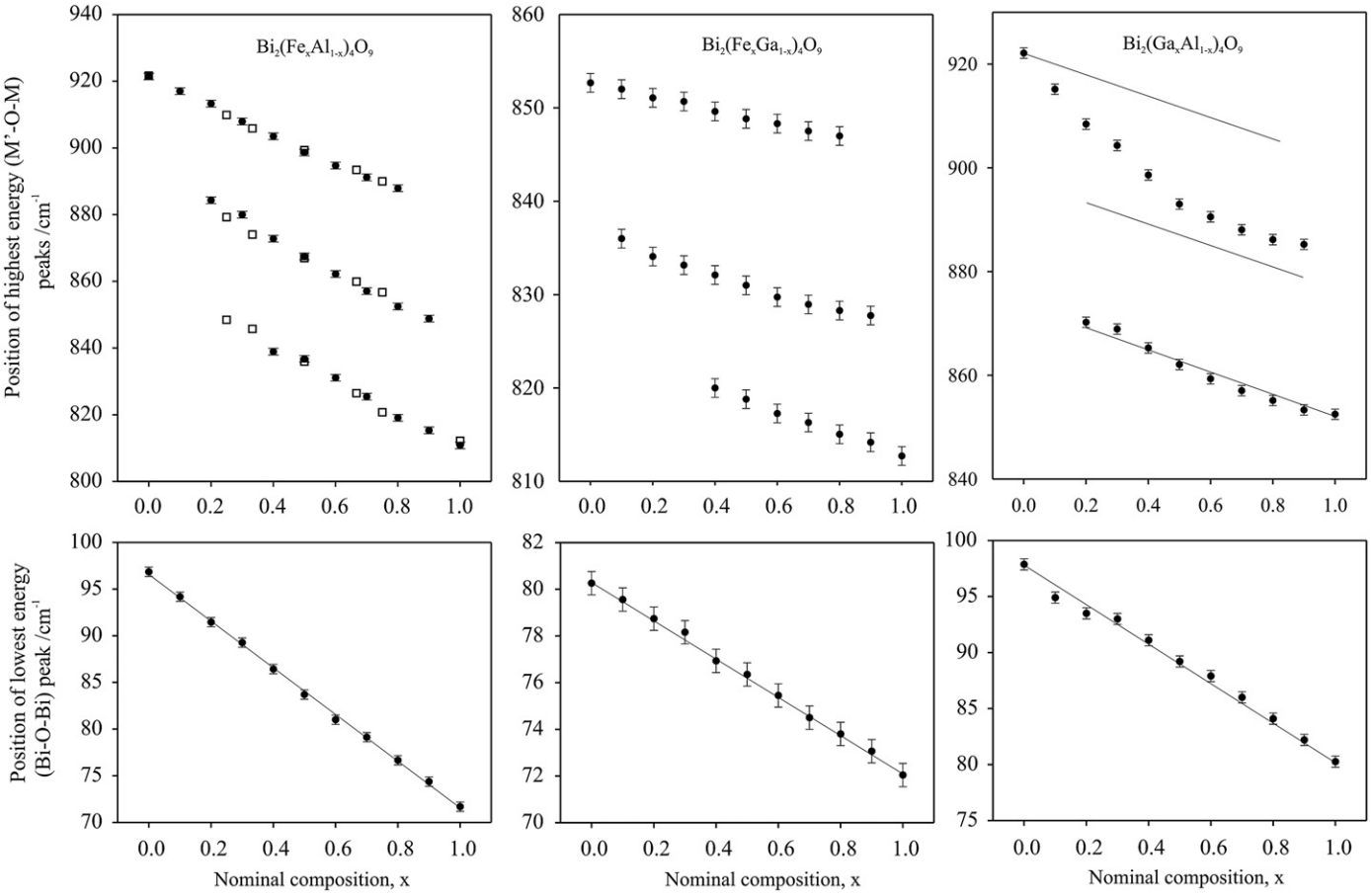

Fig. 8. Positions of peak maxima of highest frequency M–O_c–M' (M, M'=Al, Ga, Fe) and lowest frequency (Bi–O–Bi) vibrational modes as a function of M'/M (=x) ratio of the $Bi_2(M_xM'_{1-x})_4O_9$ solid-solution series.

attributed to E//c. In particular all infrared active modes superimpose in the powder spectra as claimed by Beran et al. [23] for $Bi_2Ga_4O_9$. However, any meaningful deconvolution of the powder spectra for the expected number of peaks shown in Fig. 5 between 50 and 1000 cm^{-1} might be difficult. In this sense the number of peaks observed by direct inspection might be obscured. A more complicated situation arises for the $Bi_2(M_xM'_{1-x})_4O_9$ (M, M' = Al/Ga/Fe) type compounds. The intermediate compounds of $Bi_2(Ga_xAl_{1-x})_4O_9$ and $Bi_2(Fe_xGa_{1-x})_4O_9$ solid-solution series show band shifting and splitting of the band specially in group (A), which is similar to $Bi_2(Fe_xAl_{1-x})_4O_9$ compounds [15]. Voll et al. [15] explained the triplet splitting of the band in group (A) by the presence of Al–O_c–Al, Al–O_c–Fe, and Fe–O_c–Fe bonds in the intermediate compounds of $Bi_2Al_4O_9$–$Bi_2Fe_4O_9$ solid-solution series. This kind of splitting is also observed for $Bi_2(Fe_xGa_{1-x})_4O_9$ series in the present work. But contrary to triplet splitting, absorption bands in group (A) show apparently only doublet splitting in $Bi_2(Ga_xAl_{1-x})_4O_9$ series. The peak positions of this group were measured applying the second derivative of the main IR absorption spectrum. The shift of the peak positions of this group (group A) as a function of M'/M ratio is shown in Fig. 8. Additionally, the lowest energy vibrational modes (Bi–O–Bi) of the corresponding series are shown in Fig. 8 (bottom). It can be seen that the splitted peak positions of the M'–O_c–M vibrational mode vary linearly in Fe/Al and to a good approximation linearly in Fe/Ga series. But in the case of Ga/Al series, it deviates significantly from a linear relationship. This can be explained by the overlapping of two peaks in the highest energy mode. Peak positions for Ga–O_c (in pure $Bi_2Ga_4O_9$) and Al–O_c (in pure $Bi_2Al_4O_9$) are at 852 and 922 cm^{-1}, respectively. According to this, the observed splitting of the M–O_c peak in the mixed system must be related to the different M–O_c lengths in the Al_2O_7 and Ga_2O_7 double tetrahedral units. Consequently, a third M–O_c related peak as observed for the $Bi_2(Fe_xAl_{1-x})_4O_9$ series [15] implies a third type of M–O_c bonding length, which is related to Al–O_c–Fe mixed occupation of the M_2O_7 unit and accordingly to an averaging of the two shortest bonding lengths. A third peak in the range of M–O_c vibrations of $Bi_2(Ga_xAl_{1-x})_4O_9$ mixed compositions cannot be resolved. The appearance of only two peaks and the relatively faster shift in peak positions of the M–O_c mode can be related to the predominant Ga occupancy in the tetrahedral site and to a fast disappearance of Al–O_c–Al pairs and the formation of Ga–O_c–Al pairs with increasing x. Another feature of the spectra of $Bi_2(Ga_xAl_{1-x})_4O_9$ is that there is broadening of the absorption peaks for the bands in groups (C) and (D), which may be explained by the superposition of the splitted peaks due to the local ordering of Ga–O_c–Ga and Ga–O_c–Al. The composition dependent overall shift of these peaks in all systems (Figs. 5–7) is closely related to the change in lattice parameters (Fig. 2) as predicted by the Mode–Grüneisen relationship. This relationship is most clearly observed for the peak related to Bi–O vibration (Fig. 8, bottom), which indicates a gradual change in bond length.

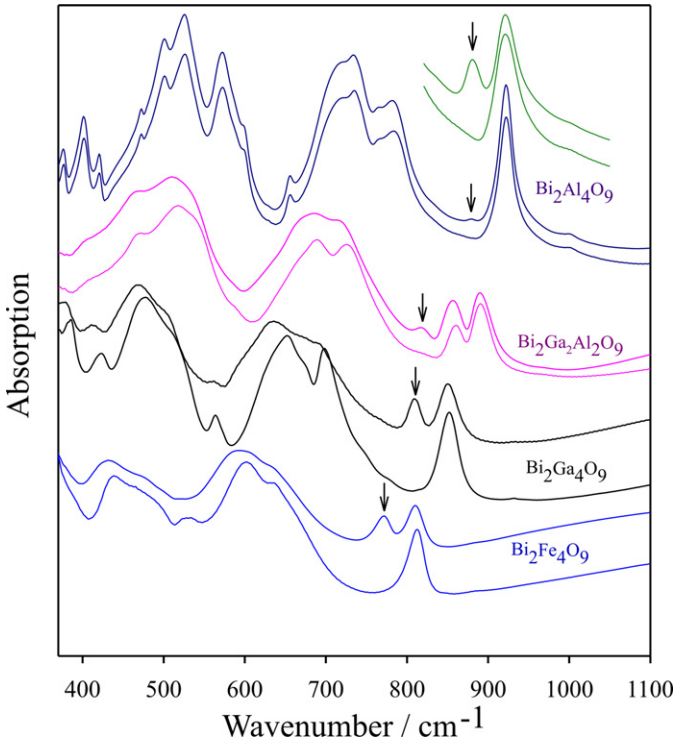

Fig. 9. IR absorption spectra of samples (as denoted) before and after $^{18}O_2$ treatment. The M–$^{18}O_c$ peaks are marked by an arrow. Spectra of 2nd $Bi_2Al_4O_9$ sample with smaller crystal size are also compared (top) (compare text and Table 3 for further details).

Table 3
Diffusion coefficients (D) of $^{18}O_2$ treated samples (16 h, 800 °C, 200 mbar 95% $^{18}O_2$), estimated using the ratio (R) of IR absorption intensity of M–$^{18}O_c$/M–$^{16}O_c$ peaks, and average crystal size (d/2) assuming spherical shape. z=^{18}O exchanged outer layer thickness.

Compositions	Average crystal size (d/2)/nm	R=M–$^{18}O_c$/M–$^{16}O_c$	z/nm	D/m^2/s
$Bi_2Ga_4O_9$	197	0.62	54.2	1.6×10^{-20}
$Bi_2Fe_4O_9$	113	0.67	34.8	5.0×10^{-21}
(a) $Bi_2Al_4O_9$	196	0.05	3.5	1.7×10^{-22}
(b) $Bi_2Al_4O_9$	35	0.39	5.3	2.3×10^{-22}
$Bi_2Ga_2Al_2O_9$	168	0.20	12.0	1.7×10^{-21}

3.3. $^{18}O/^{16}O$ exchange experiments

In Fig. 9, the IR absorption spectra of $^{18}O_2$-treated samples $Bi_2Fe_4O_9$ and $Bi_2(Ga_xAl_{1-x})_4O_9$ (x=0.0, 0.5 and 1.0) are compared with the spectra obtained before treatment. The spectra obtained for a second x=0.0 sample of significantly smaller crystal size are shown for comparison in the relevant spectral range (compare Table 3). It is observed that a thermal treatment in $^{18}O_2$ reveals an additional peak (marked by arrow), which can be assigned to the vibration of the structure specific short M–$^{18}O_c$ bonding within the double tetrahedral unit, M_2O_7. The isotopic shift of M–$^{18}O_c$ can be calculated using the measured value of the M–$^{16}O_c$ peak and the following relation: $\upsilon_{M-}{}^{18}O=\upsilon_{M-}{}^{16}O(\mu_{M-}{}^{16}O/\mu_{M-}{}^{18}O)^{1/2}$, where υ_{M-O} and μ_{M-O} represent the peak position and the reduced mass of M–O, respectively. The peak positions for Ga–$^{18}O_c$, Al–$^{18}O_c$ and Fe–$^{18}O_c$ are 810, 881 and 771 cm^{-1}, respectively, i.e. about 41 cm^{-1} lower compared to the appropriate peaks for Ga–$^{16}O_c$ (852 cm^{-1}), Al–$^{16}O_c$ (922 cm^{-1}) and Fe–$^{16}O_c$ (812 cm^{-1}). The extra peak observed for the mixed compound $Bi_2Ga_2Al_2O_9$ can be assigned to Ga–$^{18}O_c$ vibrations. Vibration due to Al–$^{18}O_c$–Ga stretching mode overlaps as low frequency shoulder to the Ga–O_c–Ga related peak.

The overall shift of the spectral weight to lower wavenumbers indicates that O_c is not the only oxygen site involved in the oxygen diffusion. However, the well separated M–$^{18}O_c$ related peak in the IR absorption spectra enables an easy estimate of the O_c-related diffusion coefficient. For this, the average crystal sizes calculated from XRD data are given in Table 3 together with the estimated relative peak intensities M–$^{18}O_c$/M–$^{16}O_c$. Assuming spherical crystals and the intensity ratio proportional to the volume ratio of the unexchanged and the exchanged part of

the crystals, the thickness of the exchanged outer shell z and the diffusion coefficients ($z=(Dt)^{1/2}$, $t=57{,}600$ s) were calculated as given in Table 3. It is observed that the estimated diffusion coefficients of powder samples $Bi_2Al_4O_9$, $Bi_2Fe_4O_9$, $Bi_2(Ga/Al)_4O_9$ and $Bi_2Ga_4O_9$ are 4–6 orders of magnitude higher than in mullite ($D=6.2\times10^{-26}$ m^{2}s^{-1}), obtained from the linear extrapolation at 800 °C of diffusion data from Refs. [24,25].

4. Summary and conclusion

New solid-solution series with compositions $Bi_2(Ga_xAl_{1-x})_4O_9$ have been prepared using amorphous gels obtained from a solution of corresponding metal nitrates in glycerine. As observed in the related systems $Bi_2(Fe_xAl_{1-x})_4O_9$ and $Bi_2(Fe_xGa_{1-x})_4O_9$ the lattice parameters of $Bi_2(Ga_xAl_{1-x})_4O_9$ series change linearly as a function of composition x. Rietveld structure refinements indicate a preferred Ga occupation on the tetrahedral site (4 h site), i.e. non-statistical distribution of Ga and Al. The effect of varying Ga/Al, Ga/Fe and Al/Fe contents was observed in the infrared spectra in particular by the systematic shift in positions of absorption bands. The position of the well-separated peak below 100 cm^{-1} as assigned to O–Bi–O bending and the high-frequency mode related to M–O_c vibrations can be used to determine the composition in the quasi-binary systems. The doublet peak splitting or non-linear peak shift in the $Bi_2(Ga_xAl_{1-x})_4O_9$ system indicates the preferred formation of Ga–O_c–Al and Ga–O_c–Ga dimers compared to Al–O_c–Al. Samples examined by $^{18}O/^{16}O$ exchange experiments show extra absorption peaks related to M–$^{18}O_c$ vibrations, which are well separated in the spectra. The intensity ratios M–$^{18}O_c/M$–$^{16}O_c$ together with the average crystal size obtained from XRD data were used to estimate the oxygen tracer diffusion coefficients as given in Table 3.

Acknowledgments

The authors thank 'Deutsche Forschungsgemainschaft' (DFG) for financial support (PAK 279).

References

[1] N. Niizeki, M. Wachi, Z. Kristallogr. 127 (1968) 173–187.
[2] A.G. Tutov, V.N. Markin, Neorg. Mater. 6 (1970) 2014–2017.
[3] H. Müller-Buschbaum, D.C. de Beaulieu, Z. Naturforsch. B Chem. Sci. 33 (1978) 669–670.
[4] R.X. Fischer, H. Schneider, in: H. Schneider, S. Komarneni (Eds.), Mullite, Wiley-VCH, Weinheim2005, pp. 1–140.
[5] L. Lopez-De-La-Torre, A. Friedrich, E.A. Juarez-Arellano, B. Winkler, D.J. Wilson, L. Bayarjargal, M. Hanfland, M. Burianek, M. Mühlberg, H. Schneider, J. Solid State Chem. 182 (2009) 767–777.
[6] G. Blasse, O.B. Ho, J. Lumin. 21 (1980) 165–168.
[7] V.V. Volkov, A.V. Egorysheva, Opt. Mater. 5 (1996) 273–277.
[8] V.V. Volkov, A.V. Egorysheva, Y.F. Kargin, V.I. Solomonov, S.G. Mikhailov, S.I. Buzmakova, B.V. Shul'gin, V.M. Skorikov, Inorg. Mater. 32 (1996) 455–458.
[9] I. Bloom, M.C. Hash, J.P. Zebrowski, K.M. Myles, M. Krumpelt, Solid State Ionics 53–56 (1992) 739–747.
[10] S.K. Filatov, S.V. Krivovichev, Y.V. Aleksandrova, R.S. Bubnova, A.V. Egorysheva, P. Burns, Y.F. Kargin, V.V. Volkov, Russ. J. Inorg. Chem. 51 (2006) 878–883.
[11] I. Abrahams, A.J. Bush, G.E. Hawkes, T. Nunes, J. Solid State Chem. 147 (1999) 631–636.
[12] D.M. Giaquinta, G.C. Papaethymiou, W.M. Davis, H.-C. zur Loye, J. Solid State Chem. 99 (1992) 120–133.
[13] D.M. Giaquinta, G.C. Papaefthymiou, H. - C. zur Loye, J. Solid State Chem. 114 (1995) 199–205.
[14] A.A. Belik, T. Wuernisha, T. Kamiyama, K. Mori, M. Maie, T. Nagai, Y. Matsui, E. Takayama-Muromachi, Chem. Matter. 18 (2006) 133–139.
[15] D. Voll, A. Beran, H. Schneider, Phys. Chem, Minerals 33 (2006) 623–628.
[16] C.H. Rüscher, T. Debnath, P. Fielitz, S. Ohmann, G. Borchardt, Diffusion Fundamentals 11 (2009), pp. 9.1–9.2.
[17] T. Debnath, C.H Rüscher , P. Fielitz, S. Ohmann, G. Borchardt, Ceramic Transactions, Design, Developments and Applications of Engineering Ceramics and Composites Vol. 215 (2010) (in press).
[18] T. Debnath, C.H. Rüscher, Z. Kristallogr., NCS. 225 (2010) 1–2.
[19] S. Larose, S.A. Akbar, J. Solid State Electrochem. 10 (2006) 488–498.
[20] S.W. Zha, J.G. Cheng, Y. Liu, X.G. Liu, G.Y. Meng, Solid State Ionics 156 (2003) 197–200.
[21] Th.M. Gesing, C.H. Rüscher, J.-Chr. Buhl, Z. Kristallogr. Suppl. 29 (2009) 93.
[22] K.J.D. MacKenzie, T. Dougherty, J. Barrel, J. Eur. Ceram. Soc. 28 (2008) 499–504.
[23] A. Beran, E. Libowitzky, M. Burianek, M. Mühlberg, C. Pecharroman, H. Schneider, Cryst. Res. Technol. 43 (2008) 1230–1239.
[24] P. Fielitz, G. Borchardt, M. Schmücker, H. Schneider, M. Wiedenbeck, D. Rhede, S. Weber, S. Scherrer, J. Am. Ceram. Soc. 84 (2001) 2845–2848.
[25] Y. Ikuma, E. Shimada, S. Sakano, M. Oishi, M. Yokoyama, Z.E. Nakagawa, J. Electrochem. Soc. 145 (1999) 4672–4675.